Vaccination with mycobacterial lipid loaded nanoparticle leads to lipid antigen persistence and memory differentiation of antigen-specific T cells

Eva Morgun,[1] Jennifer Zhu,[2] Sultan Almunif,[2] Sharan Bobbala,[2, †], Melissa S. Aguilar,[3] Junzhong Wang, [1, ‡] Kathleen Conner, [1] Yongyong Cui, [1] Liang Cao,[1] Chetan Seshadri,[3] Evan A. Scott,[1,2]* Chyung-Ru Wang[1]*

[1]Department of Microbiology and Immunology, Feinberg School of Medicine, Northwestern University, Chicago, IL, USA

[2]Department of Biomedical Engineering, Northwestern University, Evanston, IL, USA

[3]Department of Medicine, University of Washington School of Medicine, Seattle, WA, USA

Present addresses

[†] Department of Pharmaceutical Sciences, School of Pharmacy, West Virginia University, Morgantown, WV, USA

[‡]Department of Infectious Disease, Union Hospital of Tongji Medical College, Huazhong University of Science and Technology, Wuhan, China

***Corresponding authors:** Dr. Chyung-Ru Wang (chyung-ru-wang@northwestern.edu)

Dr. Evan A Scott (evan.scott@northwestern.edu)

Running title: Nanoparticle encapsulated lipid elicits antigen persistence

Keywords: nanoparticle, antigen persistence, CD1, mycolic acid, T cell, vaccination, *Mycobacterium tuberculosis*

Abstract

Mycobacterium tuberculosis (Mtb) infection elicits both protein and lipid antigen-specific T cell responses. However, the incorporation of lipid antigens into subunit vaccine strategies and formulations has been under-explored, and the properties of vaccine-induced Mtb lipid-specific memory T cells have remained elusive. Mycolic acid (MA), a major lipid component of the Mtb cell wall, is presented by human CD1b molecules to unconventional T cell subsets. These MA-specific CD1b-restricted T cells have been detected in the blood and disease sites of Mtb-infected individuals, suggesting that MA is a promising lipid antigen for incorporation into multicomponent subunit vaccines. In this study, we utilized the enhanced stability of bicontinuous nanospheres (BCN) to efficiently encapsulate MA for delivery *in vivo* to MA-specific T cells both alone and in combination with an immunodominant Mtb protein antigen (Ag85B). Pulmonary delivery of MA-loaded BCN (MA-BCN) elicited MA-specific T cell responses in humanized CD1 transgenic mice. Simultaneous delivery of MA and Ag85B within BCN activated both MA- and Ag85B-specific T cells. Interestingly, pulmonary vaccination with MA-Ag85B-BCN led to the persistence of MA, but not Ag85B, within alveolar macrophages in the lung. Vaccination of MA-BCN through intravenous or subcutaneous route, or with attenuated Mtb likewise reproduced MA persistence. Moreover, MA-specific T cells in MA-BCN-vaccinated mice differentiated into a T follicular helper-like phenotype. Overall, the BCN platform allows for the dual encapsulation and *in vivo* activation of lipid and protein antigen-specific T cells and leads to persistent lipid depots that could offer long-lasting immune responses.

Introduction

Vaccination is currently the most effective method for the prevention and eradication of infectious diseases. These efforts have been enhanced by the development of subunit vaccine formulations that include only immunodominant antigens from pathogens paired with select adjuvants. In contrast to attenuated and inactivated vaccines that contain diverse molecular components of pathogens, subunit vaccines are often preferred due to their simplicity, safety, stability, and scalability of production [1]. Yet the development of effective vaccines for several key endemic parasitic and bacterial pathogens has remained elusive. Antigen selection for subunit vaccines has thus far focused on protein molecules, overlooking a vast family of non-protein antigens such as lipids/glycolipids, metabolites, and phosphoantigens, which can be found on and within pathogens and can be recognized by various subsets of unconventional T cells [2].

Persistent antigen exposure is known to occur naturally after infection through antigen archiving by follicular dendritic cells (FDCs), which periodically present antigen to cognate B cells and aid in affinity maturation and somatic hypermutation [3, 4]. Antigen persistence can also support the maintenance of T cell response through the periodic priming of circulating T cells [5-10]. Subcutaneous vaccination has also been shown to lead to archiving of protein antigens within lymphatic endothelial cells (LECs), which induce the development of protective T cell immunity [11, 12]. However, little is known about how other vaccination routes and vaccine formulations may affect antigen archiving and persistence.

Lipid and glycolipid antigens can be presented by group 1 (CD1a, b, and c) and group 2 (CD1d) CD1 molecules to CD1-restricted T cells. Unlike MHC molecules, CD1 molecules exhibit limited polymorphism [13]. Therefore, CD1-restricted microbial lipid antigens are likely to be recognized by most individuals, making them attractive targets for vaccine development [14]. Group 1 CD1-restricted T cells have diverse T cell receptors and can recognize a variety of lipid and glycolipid antigens [15]. Microbial lipid-specific group 1 CD1-restricted T cells have been identified from several pathogens, including Mtb and other mycobacterial species: *Staphylococcus aureus* (SA), *Borrelia*

burgdorferi, *Salmonella typhimurium*, and *Brucella melitensis [15]*. CD1b-restricted T cells specific to Mtb lipids including mycolic acid (MA), an immunodominant lipid antigen[16] and component of the mycobacterial cell wall, have been identified in patients with tuberculosis (TB) [17, 18]. As group 1 CD1 molecules are not expressed in mice, we have previously developed a human CD1 transgenic mouse model (hCD1Tg). [19] Using hCD1Tg mice, we have shown that transgenic CD1b-restricted DN1 T cells specific for MA could protect against Mtb infection [20], making these potential antigens of interest in a subunit vaccine against TB.

The primary goal of a vaccine is to induce the differentiation of the adaptive immune system such that upon re-exposure to the antigen, a faster and larger response occurs, halting pathogen spread. While conventional T cells and B cells are known to undergo this differentiation, unconventional T cells such as NKT cells do not possess a comparable memory phenotype. The presence of Mtb lipid-specific group 1 CD1-restricted memory T cells has been described in both human and mice [17-19]. However, the properties of memory group 1 CD1-restricted T cells, which share similar developmental pathway as NKT cells, are not known.

Lipid antigens are difficult to formulate and administer due to their hydrophobic nature. To assess the utility of MA as a component of a subunit vaccine, we previously encapsulated MA in poly(ethylene glycol)-block-poly(propylene sulfide) (PEG-*b*-PPS) micellar nanocarriers (MA-MC) [21]. Nanocarriers composed of PEG-*b*-PPS possess several unique benefits compared to other delivery platforms, including high stability in aqueous solution [22], minimal background immunostimulation [23], and triggered release of cargo when exposed to physiological levels of reactive oxygen species [24-26]. We showed MA-MC could effectively activate adoptively transferred DN1 T cells and elicit polyclonal group 1 CD1-restricted T cell response in hCD1Tg mice after intranasal delivery [21]. While effective for stable loading of lipophilic and amphiphilic payloads, micellar nanocarriers, do not allow for facile encapsulation of hydrophilic payloads like protein antigens.

Here, we build upon our prior lipid antigen vaccine formulation by employing a nanocarrier platform engineered for the dual loading of both lipid and protein antigens. Bicontinuous nanospheres

(BCN) are polymeric analogs to lipid cubosomes and thus possess a highly organized internal cubic organization containing both intertwined hydrophobic bilayers for lipid loading as well as hydrophilic aqueous channels for protein loading [27]. Using the flash nanoprecipitation (FNP) technique [28, 29], we fabricated MA-loaded BCN (MA-BCN) and found them to have superior stimulatory capacity *in vivo* compared to MA loaded poly(D,L-lactide-co-glycolide) (PLGA) nanocarriers (MA-PLGA), which is a widely used nanocarrier platform for Mtb vaccine development [30, 31]. Furthermore, we found that after MA-BCN vaccination, MA could persist for 6 weeks post-vaccination within alveolar macrophages, a phenomenon which was dependent on the presence of an encapsulating vector, nanocarrier or bacterial, but not the route of vaccination. Due to the enhanced stability of the BCN architecture that can support the loading of diverse and multiple payloads [22, 32], we were able to efficiently co-encapsulate within BCN both MA and Ag85B, an immunodominant protein antigen of Mtb [33]. Interestingly, while both antigens activated their corresponding antigen-specific T cells, only MA resulted in antigen persistence, suggesting a potentially unique characteristic of subunit vaccines containing lipid antigens.

Results

BCN morphology preserved after MA loading

We scalably assembled spherical BCN with and without loaded MA using flash nanoprecipitation (FNP) as previously described [29]. Dynamic light scattering (DLS) showed that both MA-BCN and BCN were consistent in size (364 ±19 nm and 354 ± 14 nm, respectively), and were monodisperse based on their polydispersity indices (PDIs) of 0.24 ± 0.04 and 0.21 ±0.05, respectively (**Fig 1A**). We next verified that the BCN formulation maintained its characteristic interconnected aqueous channels using cryogenic transmission electronic microscopy (cryo-TEM) (**Fig 1B**) and negative staining transmission electron microscopy (TEM) (**Fig 1C**). Using small angle X-ray scattering (SAXS) studies, we confirmed the internal cubic organization of BCN. Bragg peaks at the $\sqrt{2}$, $\sqrt{4}$, and $\sqrt{6}$ ratios show that the primitive type of cubic internal organization was preserved between MA-BCNs and BCNs (**Fig 1D**). Thus, MA encapsulation did not disturb the BCN architecture. We also manufactured a PLGA nanocarrier formulation (PLGA-NP) with and without MA encapsulation. PLGA-NP morphology were confirmed using cryoTEM (**Suppl Fig 1A**) and SAXS (**Suppl Fig 1B**) and the size of blank PLGA-NP and MA-loaded PLGA-NP (MA-PLGA) were found to be 169 ± 4 and 163 ± 5 nm, respectively, with PDIs of 0.18 ± 0.04 and 0.19 ± 0.12, respectively (**Fig 1E**). Using the coumarin derivatization method [21], we found that BCNs could more efficiently encapsulate MA than PLGA-NPs (**Fig 1F**). We previously noted that the highly stable cubic architecture of BCN can lead to the retention of cargo within the endolysosomal compartment [22]. Indeed, Texas Red-Dextran loaded BCN were mostly found in lysosomes while Texas Red-Dextran loaded PLGA-NP could be found both within the lysosome and cytosol of cells (**Supp Fig 2A, B**).

MA-BCN activate MA-specific T cells *in vitro* and *in vivo*

As PLGA has served as a component of a wide range of vaccine formulations, including Mtb vaccines [30, 31], we benchmarked PEG-*b*-PPS BCN against PLGA-NP as a nanocarrier platform for lipid antigens. Both MA-BCN and MA-PLGA were highly effective in activating both mouse (DN1)

and human (M11) MA-specific T cells *in vitro* and inducing IFN-γ production (**Fig 2A-D**). In particular, MA-BCN were significantly better at activating MA-specific T cells compared to free MA at equivalent concentrations (**Fig 2A, B and D**). In comparison to MA-BCN, MA-PLGA was significantly more effective at stimulating mouse MA-specific T cells *in vitro* at lower concentrations. Interestingly, even in the absence of MA, PLGA-NP showed strong stimulation particularly for M11 T cells. These results demonstrate that MA encapsulation within BCN enhances its ability to stimulate antigen-specific T cells and reveal a considerable background, and thus difficult to control, stimulatory effect of blank PLGA-NP. In contrast, blank BCN showed little background immunostimulation [23], allowing a more controlled dose-dependent increase in T cell responses as the loaded MA concentration increased.

We next tested the ability of MA-loaded and unloaded BCN and PLGA to stimulate DN1 T cells *in vivo*. Intranasal (IN) vaccination of hCD1Tg mice was followed by the adoptive transfer of DN1 T cells. Surprisingly, we found that vaccination with MA-BCN induced a significantly higher percent of proliferation and activation in DN1 T cells than MA-PLGA in the draining lymph nodes (LN) and lungs at 1 week post-vaccination (**Fig 2E-G**). The extent of cell proliferation induced by MA-PLGA was not significantly different from that of blank PLGA (**Fig 2F**). Since MA-BCN effectively stimulated MA-specific T cells *in vivo* while MA-PLGA did not, we focused on further characterizing and assessing vaccination via solely MA-BCN formulations.

MA persists while Ag85B does not after vaccination with Ag85B-MA-BCN

Given the lack of knowledge regarding BCN and lipid antigen kinetics, it would be of interest to test whether delivered antigen could persist in the mouse weeks post-vaccination (**Fig 3A**). We switched from intranasal vaccination to intratracheal (IT) vaccination, as it allowed for the reliable delivery of a larger volume of the vaccine. We found that a significant proportion of the adoptively transferred DN1 T cells could proliferate and become activated in the LNs, lung, and spleen of MA-BCN-vaccinated mice 6 weeks post vaccination (**Fig 3B-D**). This activation and proliferation were

MA-specific, as no activation and proliferation of Ag85B-specific p25 Tg (p25) T cells were observed[34].

Since BCN allow for the co-loading of lipid and protein antigens, we assessed the ability of dual loaded Ag85B-MA-BCN to activate antigen-specific T cells as well as lead to antigen persistence. We co-loaded Ag85B and MA in BCN and found Ag85B-MA-BCN to have a diameter of 380 nm and PDI of 0.223, comparable to MA-BCN (**Fig 4A**). Encapsulation efficiency was also relatively high at 70%.Vaccination of hCD1Tg mice with Ag85B-MA-BCN activated and induced proliferation of both p25 and DN1 T cells in the LN, lung, and spleen (**Fig 4B-D**) at one-week post-vaccination. In addition, DN1 T cells were still able to be activated 6 weeks post-vaccination in the context of an Ag85B-MA-BCN vaccination, while p25 T cells did not show increased activation or proliferation compared to blank BCN control at this time point (**Fig 4E-H**). Therefore, MA, but not Ag85B, appears to persist in the context of an Ag85B-MA-BCN vaccination.

MA persistence was dependent on encapsulation but not route of delivery or delivery vector

To determine whether BCN encapsulation contributed to MA persistence, we designed an experiment that would allow direct comparison between MA-BCN and free MA. To account for their differential efficiency in stimulating DN1 T cells, we pulsed bone marrow-derived dendritic cells (BMDCs) from hCD1Tg mice with MA or MA-BCN at 10 μg/mL and 5 μg/mL MA concentration, respectively (**Fig 5A**). hCD1Tg mice were immunized with MA or MA-BCN-pulsed BMDCs at either 1 week or 6 weeks before the adoptive transfer of DN1 T cells, allowing comparison of short-term *vs.* long-term vaccination conditions. We found that while there were no significant differences in DN1 T cell activation and proliferation between mice vaccinated with free MA and MA-BCN pulsed BMDCs at 1-week post-vaccination, after 6 weeks, DN1 T cell response could only be detected in the MA-BCN vaccination condition (**Fig 5B, C**). Thus, BCN encapsulation contributed to the persistence of MA. We then tested whether the BCN structure could contribute to antigen persistence by comparing PEG-*b*-PPS BCNs to PEG-*b*-PPS MCs using a similar experimental set up (**Suppl Fig 3**). We found that MA-BCN and MA-MC overall had similar ability to activate DN1 T cells in both short-term and long-term

vaccination time points (**Suppl Fig 3B, C**). Thus, the structure of the encapsulating NP did not play a significant role in antigen persistence of MA.

To investigate if the IT route of vaccination played a role in the development of antigen persistence, we tested intravenous (IV) and subcutaneous (SC) vaccination routes with MA-BCN. DN1 T cell activation and proliferation were detected at 6-weeks post-vaccination through both routes of vaccination (**Fig 5D-F**), suggesting that the antigen persistence is not unique to IT vaccination. To assess whether Mtb lipid antigen persistence could also be observed in mice vaccinated with an attenuated strain of Mtb, we vaccinated hCD1Tg mice SC with Mtb $mc^2$6206 strain and tested for the persistence of both Ag85B and MA after 6 weeks. The Mtb $mc^2$6206 strain displays less virulence in mouse studies than BCG but still confers long-term protection against virulent Mtb challenge equivalent to BCG[35]. We confirmed that no bacterial burden remained at the 6 weeks time point (**Suppl Fig 4A**). Similar to MA-BCN-vaccinated mice, DN1 T cells were activated and proliferated in the draining lymph nodes and spleen of mice vaccinated with the attenuated Mtb strain (**Fig 5D-F**). In line with our findings with BCN, no proliferation was seen in p25 T cells (**Suppl Fig 4B-D**). These results suggest that incorporation of MA in a nanocarrier vaccine allows for the mimicry of the lipid antigen persistence induced by vaccination with an attenuated Mtb vaccine.

MA persists within alveolar macrophages in the lung

To identify the location of antigen persistence, we determined the biodistribution of BCN after IT vaccination using BCN loaded with the hydrophobic dye DiD (DiD-BCN). Since DiD is a lipophilic dye which, like MA, stably loads into the BCN bilayers, we could track the localization of BCN without having to perform additional chemical modifications. We found that IT-administered DiD-BCN were located almost exclusively within the lung at all time points tested (4 h, 24 h, 48 h, 6 days, and 6 weeks) (**Fig 6A**). We were able to detect fluorescence through both *in vivo* imaging system (IVIS) and flow cytometry at 6-weeks post-vaccination that was significantly above unvaccinated control (**Fig 6A, B**), despite DiD quickly losing fluorescence upon mixture into aqueous environments [36], suggesting that some DiD-BCN structure remained intact at this time point. Flow cytometric

analysis (**Suppl Fig 5**) revealed that DiD BCN was primarily found within alveolar macrophages (AMs) at both early and late time points with neutrophils and DCs showing some fluorescence at early time points (4 and 24 h) (**Fig 6C**).

We next tested whether MA likewise persisted primarily within AMs. 6-weeks after vaccination, we enriched for AMs using a column-based magnetic cell isolation system containing SiglecF antibody, which is highly expressed on AMs and a small population of eosinophils in the lung (**Fig 6D**). We co-cultured enriched AMs or the flow through with or without hCD1Tg-expressing BMDCs and DN1 T cells (**Suppl Fig 6**). While both enriched AM and flow through fractions from MA-BCN vaccinated mice co-culture with BMDCs could activate DN1 T cells (**Fig 6E**), co-culture with enriched AMs led to significantly higher DN1 T cell activation, suggesting AMs are the primary location of MA persistence. The ability of flow through to likewise lead to DN1 T cell activation suggests MA may also persist in other cell types or could be attributed to residual AMs in flow through. Furthermore, AMs could not themselves present the MA to DN1 T cells, noted by the lack of T cell activation in the absence of BMDCs, suggesting that MA may be transferred from AMs to DCs for presentation. In fact, CD1b is not expressed on AMs [19, 37] and therefore the presence of CD1b-expressing DCs may be necessary both *in vitro* and *in vivo* for T cell activation to occur. These data indicate that MA-BCN mainly persists within AMs in the lung after IT vaccination and CD1b-expressing DCs is required for antigen presentation and activation of MA-specific T cells.

Vaccination leads to DN1 T cell differentiating into T follicular helper-like T cells

To study the memory phenotype of DN1 T cells after MA-BCN vaccination, we constructed a mixed DN1 bone marrow (BM) chimera mouse model (DN1-hCD1Tg), since adoptively transferred DN1 T cells in unvaccinated mice cannot survive long term (**Fig 7A**). After vaccination, the percent of $CD44^+$ DN1 T cells in the blood increased quickly and remained high until the last time point of 40 days (**Fig 7B**). Various classical memory T cell subsets have been characterized 1 month after initial antigen-encounter, we therefore determined the DN1 T cell phenotype 6-weeks post vaccination. We found that the most prevalent memory population within DN1 T cells were $CD44^+CD62L^+$, markers

used to define central memory T cells, particularly in the LN (**Fig 7C** and **Supp Fig 7A**). To characterize the memory DN1 T cells, we performed RNA-seq analysis on sorted $CD44^{+}CD62L^{+}$ (memory) and $CD44^{-}CD62L^{+}$ (naïve) DN1 T cells from LNs of MA-BCN vaccinated DN1-hCD1Tg BM chimeric mice. We found that memory and naïve DN1 T cells clustered separately after principal component analysis (PCA), despite these samples coming from the same animals (**Suppl Fig 7B**). A total of 995 differentially expressed genes (DEGs) were identified of which 542 upregulated and 453 downregulated in the memory subset (**Suppl Fig 7C**). Next, we determined which T cell population memory DN1 T cells most resembled. Toward this end, we obtained data from ImmGen database (including terminally differentiated effector (Te), memory precursor (Tmp), central memory (Tcm), effector memory (Tem), regulatory (Treg))[42], and two additional publications (follicular helper (Tfh)[43], exhausted (Texh)[44]) and compared the respective DEG lists. Using PCA, we found that memory DN1 T cells clustered most closely to Tfh, Treg, and Texh (**Fig 7D**) and when this subset is isolated, most closely to Tfh cells (**Fig 7E**).

Within the DEGs, we noted upregulation of key Tfh cell transcription factors BCL6 and TCF1 (*TCF7*), chemokines CXCR5 and CXCR4 and surface receptor ICOS, important for Tfh cell migration into the germinal center, and adaptor protein SAP (*SH2D1A*), important for T cell-dependent B cell immunity (**Fig 7F**)[45]. Inhibitory receptors PD-1 (*PDCD1*), TIGIT, CTLA4, and transcription factor EOMES, which are known to be expressed on Tfh cells were also upregulated. In addition, we observed downregulation of transcription factor KLF2, which can inhibit Tfh cell differentiation, and CCR7 and IL-7R, receptors known to have decreased expression in T_{FH} cells. Consistent with our transcriptome analysis, we found increased percentage of $CXCR5^{+}PD\text{-}1^{+}$ DN1 T cells in MA-BCN vaccinated mice 6 weeks post-immunization (**Fig 7G, H**). Both our transcriptomic and experimental data highlighted that memory, but not naïve DN1 T cells, were proliferating, given the enrichment for the mitotic cell cycle process (**Fig 7I**) and increased $KI67^{+}$ percentage within this population (**Fig 7J**). MA-BCN vaccination thus led to the differentiation of DN1 T cells into a proliferating Tfh-like T cell population.

Discussion

Research on the development of subunit vaccines containing lipid antigens is limited. This is in part due to a lack of research into appropriate lipid vaccine formulations and their associated properties. Some early evidence suggests that lipid vaccines could contribute to protection in Mtb challenge in guinea pig model [38, 39], which naturally express group 1 CD1 molecules [40]. Vaccination with a formulation composed of total Mtb lipid encapsulated within liposomes with either dimethyl-dioctadecyl-ammonium (DDA) and/or QS-21 adjuvants showed lower bacterial burden and pathology in lung and spleen compared to unvaccinated controls [38]. In another study, two Mtb lipids (diacylated sulfoglycolipids and the phosphatidylinositol dimannosides) encapsulated into liposomes formulated with DDA and trehalose dibehenate led to a decreased bacterial burden in the spleen and overall improved pathology in lung and spleen [39]. This work motivated our current study, where we used hCD1Tg mice that express human group 1 CD1 molecules, including CD1b and MA-specific (DN1), as well as p25-specific T cells to investigate the use of nanocarriers coloaded with both Mtb lipid and protein antigens during vaccination.

We found that PEG-*b*-PPS BCN could effectively encapsulate MA as well as the protein antigen Ag85B to elicit activation of antigen-specific T cells in vaccinated mice (**Fig 4**). To our knowledge, this is the first time a dual protein and lipid loaded nanocarrier has been shown to effectively stimulate both lipid and peptide antigen-specific T cells simultaneously *in vivo*. PEG-*b*-PPS BCN can encapsulate both hydrophobic and hydrophilic molecules, making it an excellent platform for subunit vaccine delivery as both antigens and adjuvants can be co-loaded and delivered to the same cellular targets. Prior work on TB vaccines has shown that the inclusion of several protein antigens spanning the Mtb life cycle along with adjuvants with multiple boosts is paramount in the development of a vaccine that can provide effective protection against Mtb [30, 41]. As we have established that PEG-*b*-PPS BCN can easily incorporate a variety of payloads, future work will involve determining the optimal antigen and adjuvant combination for providing protection in a Mtb challenge experiment.

As several formulations of PLGA-NP have been approved for clinical uses [42], we compared MA encapsulated by either BCN or PLGA-NP and found that while PLGA appeared to offer greater, yet less controllable stimulation *in vitro* (**Fig 2**), BCN exhibited significantly greater efficacy *in vivo* (**Fig 2**). The result is not completely unexpected as a more fragile PLGA-NP could allow for fast intracellular release and antigen presentation *in vitro* while also leading to significant antigen loss prior to APC interaction *in vivo* [43]. Previous studies have documented PLGA's innate pro-inflammatory effects, while other studies have highlighted the absence and suppression of inflammatory response [44-46]. In contrast and as previously observed for PEG-*b*-PPS nanocarriers [23], we showed that unloaded BCN have little inflammatory effect (**Fig 2**), allowing their immunomodulation to be dictated by the properties of the loaded antigen and adjuvant. Thus, PEG-*b*-PPS is a promising polymer for the formulation of subunit vaccines.

We proceeded with a pulmonary (IN or IT) vaccination approach in this study based on emerging evidence that mucosal vaccination can induce a stronger immune response in the lung against Mtb in humans [47] and improve protection following vaccination with nanocarriers in mice [48]. We found that in the pulmonary route of vaccination, BCN primarily were taken up and remained within alveolar macrophages in the lung (**Fig 6**). In fact, the ability of nanocarriers to target alveolar macrophages or other APCs may contribute to their distinct capacity for inducing antigen persistence, which was not seen with cellular carriers such as MA-pulsed BMDCs (**Fig 5**). Alveolar macrophages are the first line of defense of the lungs, responsible for keeping alveoli sterile by taking up inhaled particles and pathogens through phagocytosis [49-51]. Targeting these cells may be particularly beneficial in a TB vaccine design since they may also be the main site of Mtb latency [52]. While MA remained within alveolar macrophages in the lung, T cell activation appeared to occur prominently within the draining lymph nodes (**Fig 2**), suggesting that either MA was transported from the lungs to lymph nodes where the presentation took place or T cells activated in the lung migrated to the lymph nodes. The first option seems most likely, as CD1b-expressing DCs are more prevalent in the lymph nodes [53]. Furthermore, in Mtb infection models, it has been previously shown that apoptotic macrophage and vesicles could deliver mycobacterial antigens to DCs that then activate cognate T

cells [54, 55]. Similarly, we showed that alveolar macrophages from MA-BCN vaccinated mice could only lead to T cell activation in the presence of BMDCs from hCD1Tg mice (**Fig 6**).

We demonstrated MA persistence in the lung 6 weeks post-vaccination using an *in vivo* antigen presentation assay with adoptive transfer of naïve MA-specific T cells. Sustained release of antigen through vaccination is thought to be key in the development of a robust adaptive immune response [56, 57]. Recently, spike protein was found within the draining lymph nodes of vaccinated human subjects 60 days after COVID-19 vaccination with mRNA-1273 or BNT162b2 [58]. In mice, pulmonary vaccination with adenovirus expressing influenza nucleoprotein supported long term maintenance of CD8 T_{RM} (resident memory) cells [59]. Unlike in this work, antigen persistence did not occur after subcutaneous vaccination, suggesting a distinct mechanism of antigen archiving. In a different vaccine model, subcutaneous administration of ovalbumin paired with adjuvants polyI:C and anti-CD40 led to antigen archiving by LECs [11, 12]. Similar to our findings, antigen-specific T cell activation required cross-presentation by DCs [11, 60]. Both LECs and FDCs retain antigens within a non-degradative compartment [11, 61], suggesting that residual antigens in our model may similarly remain in the endosome within undigested BCN. We have previously demonstrated the enhanced stability of BCN within cell endosomes *in vitro* for extensive periods of time [22]. This possibility is corroborated by the finding that DiD, which is easily quenched in aqueous solution [36], remained fluorescent 6 weeks post-vaccination (**Fig 6**). The lack of persistence for Ag85B could be due to its leakage out from the aqueous pores of BCN, which we have observed for other proteins [29]. Peptide antigens may be modified to include a hydrophobic tail for stable retention within BCN and therefore allow for peptide antigen persistence as well. MA's extreme hydrophobic surface, which correlates with its low permeability as a part of Mtb cell wall, may also contribute to its prolonged persistence *in vivo* [62].

After infection and vaccination, peptide antigen persistence has been shown to occur through archiving by binding to CD21 receptors on follicular dendritic cells (FDCs) in lymph nodes [3, 4]. MA antigen persistence may likewise be a natural phenomenon that can occur after infections, although its detection may be difficult given the lack of available assays to detect very small amounts of lipid antigen. T cells may, in fact, be more sensitive than any commercially available tool. While we

356 determined that MA persists within alveolar macrophages after pulmonary vaccination, the exact
357 location of persistence after SC, IV, or attenuated Mtb vaccinations remains to be tested. Overall, MA
358 antigen persistence is a robust phenomenon which occurs independently of the vector and vaccine
359 route of administration, and thus may play a role in the efficacy of a variety of vaccine strategies.
360 Additional work will focus on whether lipid antigen persistence is found across the lipid family or
361 specific to lipids with certain properties.

362 The use of memory T cells in the setting of antigen persistence may be debatable, given that
363 memory response has historically referred to the adaptive immune response in the setting of antigen
364 clearance [63]. However, given that the persistence of MA occurs even in the setting of attenuated Mtb
365 vaccination, Mtb lipid-specific long-term adaptive immunity will likely naturally exist in an antigen
366 persistent environment. We found that DN1 T cells in this setting expressed key markers of Tfh cells
367 such as CXCR5, PD-1, BCL6, and TCF1 (**Fig 7**). T cells differentiate into Tfh cells through the
368 expression of master transcription factor regulator BCL6, which directs the upregulation of chemokine
369 receptors CXCR5 and CXCR4 and thus migration into the germinal center[64, 65]. In the germinal
370 center, Tfh cells provide help to B cells for affinity maturation and class switching. Other
371 unconventional T cells are known to behave similarly such as CD1d-restricted NKT cells, which can
372 acquire a Tfh phenotype and provide B cell help through both cognate and non-cognate
373 interactions[66]. Additional work will look at whether DN1 or other group 1 CD1-restricted T cells can
374 functionally act as Tfh cells to provide B cell help, as may be suggested by the existence of IgG
375 antibodies against MA and glycolipid lipoarabinomannan in TB patients [67-69].

376 While persistence of protein antigen has been shown to improve the quality of protective
377 immunity [7, 11, 70, 71], it is not yet known how lipid antigen persistence may affect the protective
378 efficacy of lipid-specific T cells. At the very least, antigen persistence increases the probability of T
379 cell/DC encounters by increasing the time that the antigen is available. Additional work will need to
380 address the function of lipid-specific T cells differentiated in antigen persistent environments. As the
381 ultimate goal of this work is to improve the efficacy of existing subunit vaccines, future work will

assess the protective capacity of lipid antigen vaccines paired with additional protein antigens and adjuvants.

Materials and Methods

Ethics statement

This study was carried out in accordance with the recommendations in the Guide for the Care and Use of Laboratory Animals of the National Institutes of Health. The protocol was approved by the Institutional Animal Care and Use Committee of Northwestern University (Protocol number: IS000011717).

Poly (ethylene glycol)-block-poly (propylene sulfide) polymer synthesis

Poly (ethylene glycol)$_{17}$-block-poly-(propylene sulfide)$_{75}$ (PEG$_{17}$-*b*-PPS$_{75}$) copolymer was synthesized as previously reported [72, 73]. Briefly, monomethoxy PEG (molecular weight=750 Da) was functionalized with mesyl chloride and substituted with thioacetate to produce a PEG acetate initiator for the polymerization for PPS.

Bicontinuous nanosphere fabrication via flash nano precipitation

BCN were produced using FNP technique as previously described[72]. In brief, PEG$_{17}$-*b*-PPS$_{75}$ BCN polymer and any hydrophobic cargo was dissolved in THF and loaded onto a syringe. The hydrophilic cargo was loaded onto a separate syringe, and both impinged against one another through the confined impingement mixer into scintillation vial. The vial was placed in a vacuum desiccator overnight to remove the organic solvent. NPs were filtered through LH-20 column with PBS as an eluent and suspended in PBS for later use. MA encapsulation efficiency was analyzed using coumarin derivatization as previously described [21]. MA was loaded at a concentration of 100 µg/mL of total BCN formulation and DiD was loaded at 5 µg/mL total BCN formulation. MA loading capacity in BCNs was 2%. To measure the encapsulation efficiency of Ag85B, Ag85B-MA-BCN were centrifuged at 10,000 g for 10 minutes. The supernatant was collected and concentrated using Amicon® Ultra-4 10K centrifugal filter devices. To determine the unencapsulated protein concentration, the supernatant was incubated with Pierce™ BCA Protein assay reagent following the

411 manufacturer protocol and the absorbance was measured at 660 nm using a SpectraMax M3 multi-
412 mode microplate reader (Molecular Devices, LLC). The percentage encapsulation efficiency was
413 calculated as a percent of encapsulated protein to the total amount of protein added. Ag85B was
414 encapsulated at a concentration of 140 µg/mL and loading capacity was found to be 2.88%.
415
416 **Poly (lactic-co-glycolic acid nanoparticle (NP) fabrication**
417 PLGA-NP were prepared by the Oil-in-Water single emulsion method. Briefly, PLGA (20 mg in 800
418 µL dichloromethane) organic phase was emulsified using an ultrasonic processor with aqueous phase
419 containing 2 mL of polyvinyl alcohol (PVA) solution (2.5% w/v) to form an emulsion. The emulsion
420 was then added dropwise into 4 mL of stirring 0.5% w/v PVA solution at room temperature to
421 evaporate the organic solvent. NPs were collected after 4 hours of stirring followed by centrifugation at
422 10,000 x g for 10 minutes. After centrifugation, NPs were washed twice with cold water to remove
423 residual PVA and redispersed in PBS. Hydrophilic (Texas red-Dextran) or hydrophobic (MA) loading
424 was performed by adding the payloads to the aqueous and organic phases, respectively.
425
426 **Nanocarrier characterization**
427 The nanocarrier size (z-average diameter) and polydispersity was measured using dynamic light
428 scattering (DLS) using a Nano 300 ZS Zetasizer (Malvern Panalytical, Malvern, U.K.). BCN and
429 PLGA morphology was visualized with cryogenic transmission electron microscopy (cryoTEM) as
430 previously detailed [21]. Transmission electron microscopy (TEM) was performed to image BCN
431 using uranyl acetate as a negative stain as previously reported [22]. BCN aggregate structure and
432 internal morphology was characterized with small angle X-ray scattering (SAXS). These studies were
433 performed at the DuPont-Northwestern-Dow Collaborative Access Team beamline at Argonne
434 National Laboratory's Advanced Photon Source with 10 keV (wavelength $\lambda = 1.24$ Å) collimated X-
435 rays, as described previously[72].
436
437 **Confocal imaging**

Confocal images of RAW 264.7 macrophages stained with lysosomal dye Lysotracker™ (green) and NucBlue™ stain (blue) following incubation with Texas Red-labeled PLGA-NP and BCN (red) for 8 hr. The cells were then imaged within a humidified chamber using a 63X oil-immersion objective on a SP5 Leica Confocal Microscope using HyD detectors and lasers. Data analysis was performed using ImageJ software.

Mouse strains

Human CD1 transgenic mice (hCD1Tg) in C57BL/6 background or MHC II-deficient background [19] and CD1b-restricted MA-specific TCR transgenic mice on $Rag^{-/-}$ background (DN1Tg/hCD1Tg/$Rag^{-/-}$) [20] were generated in our lab as previously described. P25-specific TCR transgenic mice (Jackson lab) were crossed onto $Rag^{-/-}$ background. Both males and females were used.

Antibodies and flow cytometry

For cell surface staining, cells were pre-incubated with 2.4G2 Fcγ RII/RIII blocking mAb for 15 minutes and then stained with the appropriate combinations of mAbs diluted in HBSS + 2% FBS for 30 minutes at 4°C. Cells were analyzed on a BD FACS CantoII, or Cytek Aurora Spectral Cytometer and data were processed with FlowJo software (TreeStar). The complete list of antibodies use is as follows: anti-human Vβ5.1 (LC4, Invitrogen), anti-TCRβ (H57-597, BioLegend), anti-CD44 (IM7, BioLegend), anti-Vβ11 (KT11, BioLegend), anti-CD45.2 (104, BioLegend), anti-CD45.1 (A20, BioLegend), anti-SiglecF (E50-2440, BD Bioscience), anti-CD45 (30-F11, BioLegend), anti-CD11c (N418, BioLegend), anti-CD11b (M1/70, BioLegend), anti-Ly6G (1A8, BioLegend), anti-CD19 (6D5, BioLegend), anti-NK1.1 (PK136, BioLegend), anti-CD3 (17A2, BioLegend), Zombie Red (BioLegend), anti-mouse CD185/CXCR5 (L138D7, Biolegend), anti-mouse CD279/PD-1 (29F.1A12, Biolegend), and anti-Ki67 (SolA15, Invitrogen).

***In vitro* nanoparticle and lipid titration with MA-specific DN1 T cells**

Nanoparticle and lipid titrations were performed as previously described [21]. In brief, hCD1Tg MHC $II^{-/-}$ bone marrow-derived dendritic cells (BMDCs) were pulsed with varying quantities of nanoparticle

of sonicated MA (Sigma-Aldrich, St. Louis, MO) and then co-cultured for 48 hours with DN1 T cells isolated from lymph nodes (axial, brachial, submandibular, inguinal) of DN1Tg/hCD1Tg/Rag$^{-/-}$ mice. The supernatant was used for IFN-γ enzyme-linked immunosorbent assay (ELISA) performed as described previously [21] and cells were stained for activation.

***In vitro* nanoparticle and lipid titration with human cells via ELISPOT assay**

Hydrophobic polyvinylidene fluoride 96-well plates (Millipore, Bedford, MA) were coated with anti-human IFN-γ mAb 1-D1K (Mabtech, Cincinnati, OH) diluted 1:400 in PBS (Gibco, Waltham, MA) and incubated at 4°C overnight. The following day, mAb was removed and each plate was washed and incubated at room temperature for 2 hours in the presence of media. Human monocyte-derived dendritic cells and MA-specific M11 T cells were seeded 50,000 cells and 2,000 cells per well, respectively, together with serially diluted MA and NPs. After 16-hour incubation, plates were washed and incubated with biotinylated anti-human IFN-g (7-B6-1), diluted 1:3000 in PBS + 0.5% FBS, for 4 hours. Plates were then washed with PBS 5 times and incubated for 2 hours with ExtrAvidin-Alkaline phosphatase diluted 1:1000 in PBS + 0.5% FBS. Spots were visualized after incubation with the BCIP/NBT substrate for up to 20 minutes and then imaged with ImmunoSpot reader v.2.0.

Mouse vaccination

For both intranasal (IN) and intratracheal (IT) vaccination, mice were anesthetized using inhaled isoflurane. For IN vaccination, 25 µL of liquid was administered at the nostrils of the mice for a total of 1 µg of MA per mouse. For IT vaccination, mice were administered 25 or 50 µL of liquid for a total of 2.5 µg of MA with or without 2.0 µg of Ag85B. For BMDC vaccinations, hCD1Tg BMDCs were cultured in GM-CSF and IL-4 for 5 days[74] and pulsed with MA-BCN (5 µg/mL of MA) or free MA (10 µg/mL of MA) for 24 hours. Cells were washed and resuspended in PBS and IT vaccinated at a dose of 1x10^6 BMDCs/mouse. Intravenous vaccination was administered by tail vein injection. Subcutaneous vaccination was administered between the shoulders over the neck portion of the mouse.

Vaccination with attenuated Mtb

Attenuated Mtb strain (H37Rv Δ*panCD* Δl*euCD* referred to as mc^2 6206) was kindly provided by Jacobs' Laboratory at Albert Einstein College of Medicine. Bacteria were grown as previously described in supplemented Middlebrook 7H9 media [35, 75]. Mice were vaccinated subcutaneously with $1x10^6$ CFU in 100 µL of PBS. Mycobacterial burden quantification was performed by plating serial dilutions of lung or spleen homogenate on Middlebrook 7H11 agar plates [35, 75].

T cell Adoptive transfer and cell preparation

DN1 or p25 T cells were isolated from lymph nodes of DN1Tg/hCD1Tg/$Rag^{-/-}$ or P25Tg/$Rag^{-/-}$ mice, respectively. Cells were labeled with CellTrace™ Violet reagent (Invitrogen™) as per manufacturer's instructions and $3\text{-}5x10^6$ cells were injected into hCD1Tg mice either 1 day before vaccination (short term) or 6 weeks post-vaccination (long term). On day 7 post-adoptive transfer, draining lymph nodes (axial, brachial, mediastinal), lung, and spleen were obtained. Single-cell suspensions were prepared by mechanical disruption in HBSS/2% FBS. The lung was digested with collagenase IV (1mg/ml; Sigma-Aldrich) and DNase I (30µg/ml; Sigma- Aldrich) for 30 minutes at 37°C before the disruption.

Biodistribution imaging

BCN were loaded with DiD dye (Thermo Fisher) and administered to mice IT at 4 hours, 24 hours, 48 hours, 6 days, and 6 weeks prior to the final time point, at which all mice were sacrificed and analyzed together. Lung, spleen, and draining lymph nodes were harvested and imaged using a near-IR *in vivo* Imaging System (IVIS; Center for Advanced Molecular Imaging, Northwestern University). The single-cell suspension was then prepared from indicated organs and cells were stained for flow cytometric analysis.

Alveolar macrophage enrichment and T cell co-culture

hCD1Tg mice were immunized IT with either BCN or MA-BCN (2.5 µg of MA/mouse). 6 weeks later, lungs were isolated and single-cell suspension was stained with anti-SiglecF-PE (E50-2440, BD Bioscience). SiglecF-positive cells were enriched using anti-PE MultiSort Kit (Miltenyi Biotec). $1x10^5$

flow through and AM enriched fractions were co-cultured with $1x10^5$ hCD1Tg BMDCs and $3x10^5$ DN1 T cells for 48 hours and cells were stained for the expression of activation markers.

Generation and vaccination of BM chimeras

Bone marrow cells ^{from} DN1Tg/hCD1Tg/Rag$^{-/-}$ (CD45.2) and hCD1Tg mice (CD45.1) were depleted of mature T cells using anti-Thy-1.2 (AT83.A-6) plus rabbit complement (Cedarlane Laboratories). Equal numbers of cells ($5x10^6$) were adoptively transferred into hCD1Tg (CD45.1) mice irradiated with 900 rads. After 6 weeks, BM chimeric mice were intratracheally vaccinated with either 2.5 µg of MA in MA-BCN or equivalent volume of PBS and the activation status of DN1 T cells were monitored in the blood 1-2 times per week until experiment completion.

RNA-Seq analysis

CD44$^+$CD62L$^+$ and CD44$^-$CD62L$^+$ DN1 T cells were sorted from LNs of DN1-hCD1Tg BM chimera mice vaccinated with MA-BCN at 6 weeks post vaccination by BD FACS Aria with purity >98%. RNA was extracted with RNAeasy® mini kit (Qiagen). Libraries were generated by using the Illumina Truseq preparation kit and sequenced on HiSeq4000. Reads were analyzed with Ceto pipeline (https://github.com/ebartom/NGSbartom) using STAR and HTseq for alignment on mm10 mouse genome and reading counting, as described previously [76]. Paired differential expression analysis was performed using DESeq2 to account for original mouse sourcing[77]. All downstream analysis was performed in R and figured generated using ggplot. Gene enrichment analysis was performed using Metascape [78]. Comparisons to other T cell profiles were performed using raw transcriptome data from ImmGen database[79], and two additional publications for follicular helper (T_{FH})[80], exhausted (Texh)[81]. Analysis was performed as described above to obtain gene expression fold change values relative to internal naïve condition.

Data accessibility

The data discussed in this publication have been deposited in NCBI's Gene Expression Omnibus and are accessible through GEO Series accession number GSE226075 (https://www.ncbi.nlm.nih.gov/geo/query/acc.cgi?acc=GSE226075).

Statistical analysis

Statistical analyses were performed using Prism software 9 (GraphPad software, Inc.). Multi-group comparisons were done using two-way analysis of variance (ANOVA) with significance determined by Tukey's multiple comparison. Where appropriate, outliers were identified through Grubbs method with alpha=0.05. Statistically significance denoted as ns = not significant, *p<0.05, **p<0.01, ***p<0.001, and ****p< 0.0001.

Acknowledgments

We thank Elizabeth Bartom for use of her RNASeq analysis pipeline and Michael Kleyman for his advice on comparing gene expression among multiple T cell populations. We would like to thank the Center for Advanced Molecular Imaging (CAMI) for their help in performing IVIS and The Northwestern University's Atomic and Nanoscale Characterization Experimental Center (NUANCE) Keck-II facility for their help with NP characterization. Ag85B from *Mycobacterium tuberculosis* H37Rv was obtained through BEI Resources, NIAID, NIH. SAXS experiments were performed at the DuPont-Northwestern-Dow Collaborative Access Team (DND-CAT) located at Sector 5 of the Advanced Photon Source. DND-CAT is supported by Northwestern University, The Dow Chemical Company, and DuPont de Nemours, Inc. This research used resources of the Advanced Photon Source; a U.S. Department of Energy (DOE) Office of Science User Facility operated for the DOE Office of Science by Argonne National Laboratory under Contract No. DE-AC02-06CH11357. Data was collected using an instrument funded by the National Science Foundation under Award No. 0960140.

Funding:

This work was supported by the following grans:

National Institutes of Health grant R01AI057460 (CRW), R01AI145345 (CRW, EAS)

National Institutes of Health grant F30AI157314 (EM)

National Institutes of Health grant T32GM008152 (EM)

National Institutes of Health grant R01AI146072 (CS)

Competing interests: Authors declare that they have no competing financial interests.

Data and materials availability:

All data are available in the main text or the supplementary materials. Derived data supporting the findings of this study are available from the corresponding author CRW and EAS on request. Generated transgenic mice and nanoparticles are available upon request upon signing of Material Transfer Agreement (MTA).

Nonstandard Abbreviations:

Mtb, *Mycobacterium tuberculosis*; MA, mycolic acid; BCN, bicontinuous nanospheres; MA-BCN, mycolic acid loaded bicontinuous nanospheres; FDCs, follicular dendritic cells; LECs, lymphocytic endothelial cells; hCD1Tg, human CD1 transgenic mouse model; APCs, antigen-presenting cells; PEG-b-PPS, poly(ethylene glycol)-block-poly(propylene sulfide); MA-MC, mycolic acid loaded micellar nanocarrier; FNP, flash nanoprecipitation; PLGA, poly(D,L-lactide-co-glycolide); DLS, dynamic light scattering; PDI, polydispersity index; cryo-TEM, cryogenic transmission electron microscopy; SAXS, small angle X-ray scattering; PLGA-NP, poly(D,L-lactide-co-glycolide) nanoparticle; MA-PLGA, mycolic acid loaded poly(D,L-lactide-co-glycolide); IN, intranasal; IT, intratracheal; Ag85B-MA-BCN, Ag85B and mycolic acid loaded bicontinuous nanosphere; BMDCs, bone marrow-derived dendritic cells; DiD-BCN, DiD loaded bicontinuous nanosphere; AMs, alveolar macrophages.

600 **References**

601

602 1. Karch CP, Burkhard P. Vaccine technologies: From whole organisms to rationally designed
603 protein assemblies. Biochem Pharmacol. 2016;120:1-14. Epub 20160506. doi:
604 10.1016/j.bcp.2016.05.001. PubMed PMID: 27157411; PubMed Central PMCID: PMCPMC5079805.
605 2. Legoux F, Salou M, Lantz O. Unconventional or Preset alphabeta T Cells: Evolutionarily
606 Conserved Tissue-Resident T Cells Recognizing Nonpeptidic Ligands. Annu Rev Cell Dev Biol.
607 2017;33:511-35. Epub 20170629. doi: 10.1146/annurev-cellbio-100616-060725. PubMed PMID:
608 28661722.
609 3. Heesters BA, Myers RC, Carroll MC. Follicular dendritic cells: Dynamic antigen libraries.
610 Nature Publishing Group; 2014. p. 495-504.
611 4. Hirosue S, Dubrot J. Modes of antigen presentation by lymph node stromal cells and their
612 immunological implications. Frontiers in Immunology. 2015;6. doi: ARTN 446
613 10.3389/fimmu.2015.00446. PubMed PMID: WOS:000361632700001.
614 5. Takamura S, Roberts AD, Jelley-Gibbs DM, Wittmer ST, Kohlmeier JE, Woodland DL. The
615 route of priming influences the ability of respiratory virus-specific memory CD8+ T cells to be
616 activated by residual antigen. Journal of Experimental Medicine. 2010;207(6):1153-60. doi:
617 10.1084/jem.20090283.
618 6. Kim TS, Hufford MM, Sun J, Fu YX, Braciale TJ. Antigen persistence and the control of local
619 T cell memory by migrant respiratory dendritic cells after acute virus infection. Journal of
620 Experimental Medicine. 2010;207(6):1161-72. doi: 10.1084/jem.20092017.
621 7. Demento SL, Cui W, Criscione JM, Stern E, Tulipan J, Kaech SM, et al. Role of sustained
622 antigen release from nanoparticle vaccines in shaping the T cell memory phenotype. Biomaterials.
623 2012;33(19):4957-64. Epub 20120406. doi: 10.1016/j.biomaterials.2012.03.041. PubMed PMID:
624 22484047; PubMed Central PMCID: PMCPMC5724530.

625 8. Zammit DJ, Turner DL, Klonowski KD, Lefrançois L, Cauley LS. Residual Antigen
626 Presentation after Influenza Virus Infection Affects CD8 T Cell Activation and Migration. Immunity.
627 2006;24(4):439-49. doi: 10.1016/j.immuni.2006.01.015.
628 9. Woodland DL, Kohlmeier JE. Migration, maintenance and recall of memory T cells in
629 peripheral tissues. Nat Rev Immunol. 2009;9(3):153-61. doi: 10.1038/nri2496. PubMed PMID:
630 19240755.
631 10. Vokali E, Yu SS, Hirosue S, Rincon-Restrepo M, F VD, Scherer S, et al. Lymphatic endothelial
632 cells prime naive CD8(+) T cells into memory cells under steady-state conditions. Nat Commun.
633 2020;11(1):538. Epub 20200127. doi: 10.1038/s41467-019-14127-9. PubMed PMID: 31988323;
634 PubMed Central PMCID: PMCPMC6985113.
635 11. Tamburini BA, Burchill MA, Kedl RM. Antigen capture and archiving by lymphatic
636 endothelial cells following vaccination or viral infection. Nature Communications. 2014;5(1):3989-.
637 doi: 10.1038/ncomms4989.
638 12. Walsh SM, Sheridan RM, Lucas ED, Doan TA, Ware BC, Schafer J, et al. Molecular tracking
639 devices quantify antigen distribution and archiving in the murine lymph node. Elife. 2021;10. Epub
640 20210412. doi: 10.7554/eLife.62781. PubMed PMID: 33843587; PubMed Central PMCID:
641 PMCPMC8116055.
642 13. Reinink P, Van Rhijn I. Mammalian CD1 and MR1 genes. Immunogenetics. 2016;68(8):515-
643 23. Epub 20160728. doi: 10.1007/s00251-016-0926-x. PubMed PMID: 27470004; PubMed Central
644 PMCID: PMCPMC5002277.
645 14. Joosten SA, Ottenhoff THM, Lewinsohn DM, Hoft DF, Moody DB, Seshadri C. Harnessing
646 donor unrestricted T-cells for new vaccines against tuberculosis. 2019. p. 3022-30.
647 15. Morgun E, Cao LC, Wang C-R. Role of Group 1 CD1-restricted T Cells in Host Defense and
648 Inflammatory Diseases. Critical Reviews in Immunology. 2021. doi:
649 10.1615/critrevimmunol.2021040089.

16. Busch M, Herzmann C, Kallert S, Zimmermann A, Hofer C, Mayer D, et al. Lipoarabinomannan-responsive polycytotoxic T cells are associated with protection in human tuberculosis. American Journal of Respiratory and Critical Care Medicine. 2016;194(3):345-55. doi: 10.1164/rccm.201509-1746OC.

17. Lopez K, Iwany SK, Suliman S, Reijneveld JF, Ocampo TA, Jimenez J, et al. CD1b Tetramers Broadly Detect T Cells That Correlate With Mycobacterial Exposure but Not Tuberculosis Disease State. Frontiers in Immunology. 2020;11:199-. doi: 10.3389/fimmu.2020.00199.

18. Montamat-Sicotte DJ, Millington KA, Willcox CR, Hingley-Wilson S, Hackforth S, Innes J, et al. A mycolic acid-specific CD1-restricted T cell population contributes to acute and memory immune responses in human tuberculosis infection. Journal of Clinical Investigation. 2011;121(6):2493-503. doi: 10.1172/JCI46216.

19. Felio K, Nguyen H, Dascher CC, Choi H-J, Li S, Zimmer MI, et al. CD1-restricted adaptive immune responses to Mycobacteria in human group 1 CD1 transgenic mice. The Journal of experimental medicine. 2009;206(11):2497-509. doi: 10.1084/jem.20090898.

20. Zhao J, Siddiqui S, Shang S, Bian Y, Bagchi S, He Y, et al. Mycolic acid-specific T cells protect against Mycobacterium tuberculosis infection in a humanized transgenic mouse model. eLife. 2015;4. doi: 10.7554/eLife.08525.

21. Shang S, Kats D, Cao L, Morgun E, Velluto D, He Y, et al. Induction of Mycobacterium Tuberculosis Lipid-Specific T Cell Responses by Pulmonary Delivery of Mycolic Acid-Loaded Polymeric Micellar Nanocarriers. Frontiers in Immunology. 2018;9:2709-. doi: 10.3389/fimmu.2018.02709.

22. Bobbala S, Allen SD, Yi S, Vincent M, Frey M, Karabin NB, et al. Employing bicontinuous-to-micellar transitions in nanostructure morphology for on-demand photo-oxidation responsive cytosolic delivery and off-on cytotoxicity. Nanoscale. 2020;12(9):5332-40. doi: 10.1039/c9nr10921h.

674 23. Burke JA, Zhang X, Bobbala S, Frey MA, Bohorquez Fuentes C, Freire Haddad H, et al.
675 Subcutaneous nanotherapy repurposes the immunosuppressive mechanism of rapamycin to enhance
676 allogeneic islet graft viability. Nat Nanotechnol. 2022. Epub 20220117. doi: 10.1038/s41565-021-
677 01048-2. PubMed PMID: 35039683.
678 24. Du F, Liu YG, Scott EA. Immunotheranostic Polymersomes Modularly Assembled from
679 Tetrablock and Diblock Copolymers with Oxidation-Responsive Fluorescence. Cell Mol Bioeng.
680 2017;10(5):357-70. Epub 20170410. doi: 10.1007/s12195-017-0486-7. PubMed PMID: 28989540;
681 PubMed Central PMCID: PMCPMC5628512.
682 25. Scott EA, Stano A, Gillard M, Maio-Liu AC, Swartz MA, Hubbell JA. Dendritic cell activation
683 and T cell priming with adjuvant- and antigen-loaded oxidation-sensitive polymersomes. Biomaterials.
684 2012;33(26):6211-9. doi: 10.1016/j.biomaterials.2012.04.060.
685 26. Napoli A, Valentini M, Tirelli N, Müller M, Hubbell JA. Oxidation-responsive polymeric
686 vesicles. Nature Materials. 2004;3(3):183-9. doi: 10.1038/nmat1081.
687 27. Allen SD, Bobbala S, Karabin NB, Scott EA. On the advancement of polymeric bicontinuous
688 nanospheres toward biomedical applications. Nanoscale Horiz. 2019;4(2):258-72. Epub 20181120.
689 doi: 10.1039/c8nh00300a. PubMed PMID: 32254084.
690 28. Saad WS, Prud'Homme RK. Principles of nanoparticle formation by flash nanoprecipitation.
691 Nano Today. 2016;11(2):212-27. doi: 10.1016/j.nantod.2016.04.006.
692 29. Bobbala S, Allen SD, Scott EA. Flash nanoprecipitation permits versatile assembly and loading
693 of polymeric bicontinuous cubic nanospheres. Nanoscale. 2018;10(11):5078-88. doi:
694 10.1039/C7NR06779H.
695 30. Lin LCW, Chattopadhyay S, Lin JC, Hu CMJ. Advances and Opportunities in Nanoparticle-
696 and Nanomaterial-Based Vaccines against Bacterial Infections. Wiley-Blackwell; 2018. p. 1701395-.

697 31. Khademi F, Derakhshan M, Yousefi-Avarvand A, Tafaghodi M. Potential of polymeric
698 particles as future vaccine delivery systems/adjuvants for parenteral and non-parenteral immunization
699 against tuberculosis: A systematic review. Mashhad University of Medical Sciences; 2018. p. 116-23.
700 32. Modak M, Bobbala S, Lescott C, Liu YG, Nandwana V, Dravid VP, et al. Magnetic
701 Nanostructure-Loaded Bicontinuous Nanospheres Support Multicargo Intracellular Delivery and
702 Oxidation-Responsive Morphological Transitions. ACS Appl Mater Interfaces. 2020;12(50):55584-95.
703 Epub 20201201. doi: 10.1021/acsami.0c15920. PubMed PMID: 33259182.
704 33. Huygen K. The Immunodominant T-Cell Epitopes of the Mycolyl-Transferases of the Antigen
705 85 Complex of M. tuberculosis. Front Immunol. 2014;5:321. Epub 20140709. doi:
706 10.3389/fimmu.2014.00321. PubMed PMID: 25071781; PubMed Central PMCID: PMCPMC4089088.
707 34. Tamura T, Ariga H, Kinashi T, Uehara S, Kikuchi T, Nakada M, et al. The role of antigenic
708 peptide in CD4+ T helper phenotype development in a T cell receptor transgenic model. International
709 Immunology. 2004;16(12):1691-9. doi: 10.1093/intimm/dxh170.
710 35. Sampson SL, Dascher CC, Sambandamurthy VK, Russell RG, Jacobs WR, Jr., Bloom BR, et
711 al. Protection elicited by a double leucine and pantothenate auxotroph of Mycobacterium tuberculosis
712 in guinea pigs. Infect Immun. 2004;72(5):3031-7. doi: 10.1128/IAI.72.5.3031-3037.2004. PubMed
713 PMID: 15102816; PubMed Central PMCID: PMCPMC387862.
714 36. Invitrogen™. DiD' solid; DiIC18(5) solid (1,1'-Dioctadecyl-3,3,3',3'-
715 Tetramethylindodicarbocyanine, 4-Chlorobenzenesulfonate Salt).
716 37. Barral DC, Brenner MB. CD1 antigen presentation: how it works. Nature Reviews
717 Immunology. 2007;7(12):929-41. doi: 10.1038/nri2191.
718 38. Dascher CC, Hiromatsu K, Xiong X, Morehouse C, Watts G, Liu G, et al. Immunization with a
719 mycobacterial lipid vaccine improves pulmonary pathology in the guinea pig model of tuberculosis.
720 Oxford University Press; 2003. p. 915-25.

721 39. Larrouy-Maumus G, Layre E, Clark S, Prandi J, Rayner E, Lepore M, et al. Protective efficacy
722 of a lipid antigen vaccine in a guinea pig model of tuberculosis. Vaccine. 2017;35(10):1395-402. doi:
723 10.1016/J.VACCINE.2017.01.079.
724 40. Eckhardt E, Bastian M. Animal models for human group 1 CD1 protein function. Molecular
725 Immunology. 2021;130:159-63. doi: 10.1016/j.molimm.2020.12.018.
726 41. Schrager LK, Vekemens J, Drager N, Lewinsohn DM, Olesen OF. The status of tuberculosis
727 vaccine development. Lancet Infect Dis. 2020;20(3):e28-e37. Epub 20200131. doi: 10.1016/S1473-
728 3099(19)30625-5. PubMed PMID: 32014117.
729 42. Wang Y, Qin B, Xia G, Choi SH. FDA's Poly (Lactic-Co-Glycolic Acid) Research Program
730 and Regulatory Outcomes. Aaps J. 2021;23(4):92. Epub 20210629. doi: 10.1208/s12248-021-00611-y.
731 PubMed PMID: 34189655.
732 43. Ding D, Zhu Q. Recent advances of PLGA micro/nanoparticles for the delivery of
733 biomacromolecular therapeutics. Materials Science & ENgineering C. 2018. doi:
734 10.1016/j.msec.2017.12.036.
735 44. Barillet S, Fattal E, Mura S, Tsapis N, Pallardy M, Hillaireau H, et al. Immunotoxicity of poly
736 (lactic-co-glycolic acid) nanoparticles: influence of surface properties on dendritic cell activation.
737 Nanotoxicology. 2019;13(5):606-22. Epub 20190214. doi: 10.1080/17435390.2018.1564078. PubMed
738 PMID: 30760076.
739 45. Ma S, Feng X, Liu F, Wang B, Zhang H, Niu X. The pro-inflammatory response of
740 macrophages regulated by acid degradation products of poly(lactide-co-glycolide) nanoparticles. Eng
741 Life Sci. 2021;21(10):709-20. Epub 20210512. doi: 10.1002/elsc.202100040. PubMed PMID:
742 34690640; PubMed Central PMCID: PMCPMC8518582.
743 46. Nicolete R, dos Santos DF, Faccioli LH. The uptake of PLGA micro or nanoparticles by
744 macrophages provokes distinct in vitro inflammatory response. Int Immunopharmacol.
745 2011;11(10):1557-63. Epub 20110527. doi: 10.1016/j.intimp.2011.05.014. PubMed PMID: 21621649.

746 47. Stylianou E, Paul MJ, Reljic R, McShane H. Mucosal delivery of tuberculosis vaccines: a
747 review of current approaches and challenges. Expert Rev Vaccines. 2019;18(12):1271-84. Epub
748 20191226. doi: 10.1080/14760584.2019.1692657. PubMed PMID: 31876199; PubMed Central
749 PMCID: PMCPMC6961305.
750 48. Ballester M, Nembrini C, Dhar N, de Titta A, de Piano C, Pasquier M, et al. Nanoparticle
751 conjugation and pulmonary delivery enhance the protective efficacy of Ag85B and CpG against
752 tuberculosis. Vaccine. 2011;29(40):6959-66. doi: 10.1016/j.vaccine.2011.07.039. PubMed PMID:
753 WOS:000295300500018.
754 49. Fels AO, Cohn ZA. The alveolar macrophage. J Appl Physiol (1985). 1986;60(2):353-69. doi:
755 10.1152/jappl.1986.60.2.353. PubMed PMID: 3005225.
756 50. Bowden DH. The alveolar macrophage. Environ Health Perspect. 1984;55:327-41. doi:
757 10.1289/ehp.8455327. PubMed PMID: 6376105; PubMed Central PMCID: PMCPMC1568378.
758 51. Geiser M. Update on macrophage clearance of inhaled micro- and nanoparticles. J Aerosol
759 Med Pulm Drug Deliv. 2010;23(4):207-17. doi: 10.1089/jamp.2009.0797. PubMed PMID: 20109124.
760 52. Pai M, Behr MA, Dowdy D, Dheda K, Divangahi M, Boehme CC, et al. Tuberculosis. Nat Rev
761 Dis Primers. 2016;2:16076. Epub 20161027. doi: 10.1038/nrdp.2016.76. PubMed PMID: 27784885.
762 53. Dougan SK, Kaser A, Blumberg RS. CD1 Expression on Antigen-Presenting Cells. 314. Berlin,
763 Heidelberg: Springer Berlin Heidelberg; 2007. p. 113-41.
764 54. Espinosa-Cueto P, Magallanes-Puebla A, Castellanos C, Mancilla R. Dendritic cells that
765 phagocytose apoptotic macrophages loaded with mycobacterial antigens activate CD8 T cells via
766 cross-presentation. PLoS One. 2017;12(8):e0182126. Epub 20170802. doi:
767 10.1371/journal.pone.0182126. PubMed PMID: 28767693; PubMed Central PMCID:
768 PMCPMC5540487.

769 55. Schaible UE, Winau F, Sieling PA, Fischer K, Collins HL, Hagens K, et al. Apoptosis
770 facilitates antigen presentation to T lymphocytes through MHC-I and CD1 in tuberculosis. Nat Med.
771 2003;9(8):1039-46. Epub 20030720. doi: 10.1038/nm906. PubMed PMID: 12872166.
772 56. Silva AL, Soema PC, Slutter B, Ossendorp F, Jiskoot W. PLGA particulate delivery systems
773 for subunit vaccines: Linking particle properties to immunogenicity. Hum Vaccin Immunother.
774 2016;12(4):1056-69. Epub 20160111. doi: 10.1080/21645515.2015.1117714. PubMed PMID:
775 26752261; PubMed Central PMCID: PMCPMC4962933.
776 57. Correia-Pinto JF, Csaba N, Alonso MJ. Vaccine delivery carriers: insights and future
777 perspectives. Int J Pharm. 2013;440(1):27-38. Epub 20120423. doi: 10.1016/j.ijpharm.2012.04.047.
778 PubMed PMID: 22561794.
779 58. Roltgen K, Nielsen SCA, Silva O, Younes SF, Zaslavsky M, Costales C, et al. Immune
780 imprinting, breadth of variant recognition, and germinal center response in human SARS-CoV-2
781 infection and vaccination. Cell. 2022;185(6):1025-40 e14. Epub 20220125. doi:
782 10.1016/j.cell.2022.01.018. PubMed PMID: 35148837; PubMed Central PMCID: PMCPMC8786601.
783 59. Uddback I, Cartwright EK, Scholler AS, Wein AN, Hayward SL, Lobby J, et al. Long-term
784 maintenance of lung resident memory T cells is mediated by persistent antigen. Mucosal Immunol.
785 2021;14(1):92-9. Epub 20200609. doi: 10.1038/s41385-020-0309-3. PubMed PMID: 32518368;
786 PubMed Central PMCID: PMCPMC7726002.
787 60. Kedl RM, Lindsay RS, Finlon JM, Lucas ED, Friedman RS, Tamburini BAJ. Migratory
788 dendritic cells acquire and present lymphatic endothelial cell-archived antigens during lymph node
789 contraction. Nat Commun. 2017;8(1):2034. Epub 20171211. doi: 10.1038/s41467-017-02247-z.
790 PubMed PMID: 29229919; PubMed Central PMCID: PMCPMC5725486.
791 61. Heesters BA, Chatterjee P, Kim YA, Gonzalez SF, Kuligowski MP, Kirchhausen T, et al.
792 Endocytosis and recycling of immune complexes by follicular dendritic cells enhances B cell antigen
793 binding and activation. Immunity. 2013;38(6):1164-75. Epub 20130613. doi:

10.1016/j.immuni.2013.02.023. PubMed PMID: 23770227; PubMed Central PMCID: PMCPMC3773956.

62. Daffé M, Quémard A, Marrakchi H. Mycolic Acids: From Chemistry to Biology. 2019. p. 181-216.

63. Martin MD, Badovinac VP. Defining memory CD8 T cell. Frontiers Media SA; 2018.

64. Johnston RJ, Poholek AC, DiToro D, Yusuf I, Eto D, Barnett B, et al. Bcl6 and Blimp-1 are reciprocal and antagonistic regulators of T follicular helper cell differentiation. Science. 2009;325(5943):1006-10. doi: 10.1126/science.1175870.

65. Nurieva RI, Chung Y, Martinez GJ, Yang XO, Tanaka S, Matskevitch TD, et al. Bcl6 mediates the development of T follicular helper cells. Science. 2009;325(5943):1001-5. doi: 10.1126/science.1176676.

66. Clerici L, Casorati G, Dellabona P. B Cell Help by CD1d-Rectricted NKT Cells. Antibodies. 2015;4(4):279-94. doi: 10.3390/antib4040279.

67. Correia-Neves M, Sundling C, Cooper A, Kallenius G. Lipoarabinomannan in Active and Passive Protection Against Tuberculosis. Front Immunol. 2019;10:1968. Epub 20190911. doi: 10.3389/fimmu.2019.01968. PubMed PMID: 31572351; PubMed Central PMCID: PMCPMC6749014.

68. Schleicher GK, Feldman C, Vermaak Y, Verschoor JA. Prevalence of anti-mycolic acid antibodies in patients with pulmonary tuberculosis co-infected with HIV. Clinical Chemistry and Laboratory Medicine. 2002;40(9):882-7. doi: 10.1515/CCLM.2002.156.

69. Pan J, Fujiwara N, Oka S, Maekura R, Ogura T, Yano I. Anti-cord factor (trehalose 6,6'dimycolate) IgG antibody in tuberculosis patients recognizes mycolic acid subclasses. Microbiol Immunol. 1999;43(9):863-9. doi: 10.1111/j.1348-0421.1999.tb01221.x. PubMed PMID: 10553679.

70. Bioley G, Lassus A, Terrettaz J, Tranquart F, Corthésy B. Long-term persistence of immunity induced by OVA-coupled gas-filled microbubble vaccination partially protects mice against infection by OVA-expressing Listeria. Biomaterials. 2015;57:153-60. doi: 10.1016/j.biomaterials.2015.04.008.

819 71. Silva AL, Rosalia RA, Sazak A, Carstens MG, Ossendorp F, Oostendorp J, et al. Optimization
820 of encapsulation of a synthetic long peptide in PLGA nanoparticles: low-burst release is crucial for
821 efficient CD8(+) T cell activation. Eur J Pharm Biopharm. 2013;83(3):338-45. Epub 20121129. doi:
822 10.1016/j.ejpb.2012.11.006. PubMed PMID: 23201055.
823 72. Allen SD, Bobbala S, Karabin NB, Modak M, Scott EA. Benchmarking Bicontinuous
824 Nanospheres against Polymersomes for in Vivo Biodistribution and Dual Intracellular Delivery of
825 Lipophilic and Water-Soluble Payloads. ACS Applied Materials & Interfaces. 2018;10(40):33857-66.
826 doi: 10.1021/acsami.8b09906.
827 73. Frey M. Development and Optimization of Functionalized Self-Assembling Polymeric
828 Nanobiomaterials: Northwestern University; 2021.
829 74. Li S, Choi HJ, Felio K, Wang CR. Autoreactive CD1b-restricted T cells: A new innate-like T-
830 cell population that contributes to immunity against infection. Blood. 2011;118(14):3870-8. doi:
831 10.1182/blood-2011-03-341941.
832 75. Larsen MH, Biermann K, Chen B, Hsu T, Sambandamurthy VK, Lackner AA, et al. Efficacy
833 and safety of live attenuated persistent and rapidly cleared Mycobacterium tuberculosis vaccine
834 candidates in non-human primates. Vaccine. 2009;27(34):4709-17. Epub 20090602. doi:
835 10.1016/j.vaccine.2009.05.050. PubMed PMID: 19500524; PubMed Central PMCID:
836 PMCPMC3512200.
837 76. Weng X, Kumar A, Cao L, He Y, Morgun E, Visvabharathy L, et al. Mitochondrial metabolism
838 is essential for invariant natural killer T cell development and function. Proc Natl Acad Sci U S A.
839 2021;118(13). Epub 2021/03/24. doi: 10.1073/pnas.2021385118. PubMed PMID: 33753493.
840 77. Love MI, Huber W, Anders S. Moderated estimation of fold change and dispersion for RNA-
841 seq data with DESeq2. Genome Biol. 2014;15(12):550. Epub 2014/12/18. doi: 10.1186/s13059-014-
842 0550-8. PubMed PMID: 25516281; PubMed Central PMCID: PMCPMC4302049.

843 78. Zhou Y, Zhou B, Pache L, Chang M, Khodabakhshi AH, Tanaseichuk O, et al. Metascape
844 provides a biologist-oriented resource for the analysis of systems-level datasets. Nature
845 Communications. 2019;10(1). doi: 10.1038/s41467-019-09234-6.
846 79. Yoshida H, Lareau CA, Ramirez RN, Rose SA, Maier B, Wroblewska A, et al. The cis-
847 Regulatory Atlas of the Mouse Immune System. Cell. 2019;176(4):897-912.e20. doi:
848 10.1016/j.cell.2018.12.036.
849 80. Lahmann A, Kuhrau J, Fuhrmann F, Heinrich F, Bauer L, Durek P, et al. Bach2 Controls T
850 Follicular Helper Cells by Direct Repression of Bcl-6. The Journal of Immunology. 2019;202(8):2229-
851 39. doi: 10.4049/jimmunol.1801400.
852 81. Man K, Gabriel SS, Liao Y, Gloury R, Preston S, Henstridge DC, et al. Transcription Factor
853 IRF4 Promotes CD8+ T Cell Exhaustion and Limits the Development of Memory-like T Cells during
854 Chronic Infection. Immunity. 2017;47(6):1129-41.e5. doi: 10.1016/j.immuni.2017.11.021.
855

Figure Legends

Fig. 1. Physicochemical characterization of BCN and PLGA-NP. **(A)** Dynamic light scattering (DLS) analysis of blank BCN and MA-BCN. **(B)** CryoTEM of MA-BCN (scale = 500 nm). **(C)** Negative staining TEM images of MA-BCN. **(D)** SAXS of blank BCN and MA-BCN. **(E)** DLS analysis of blank PLGA and MA PLGA. **(F)** MA encapsulation efficiency for MA-BCN and MA PLGA. N = 3 per condition. Data represented as mean ± SD.

Fig. 2. MA-BCN effectively activated MA-specific T cells *in vitro* and *in vivo*. (A, B) BMDCs were pulsed for 18 hrs. with selected nanoparticles at various concentrations, co-cultured for 48 hrs. with DN1 T cells, and T cell activation was measured. **(A)** Percentage of CD69 and CD25-expressing DN1 T cells. **(B)** IFN-g production measured by ELISA. (N=3). (**C, D**) ELISPOT of IFN-g from MA-specific human M11 T cells cultured for 16 hours with monocyte-derived dendritic cells with selected nanoparticles at high **(C)** and low **(D)** concentrations. Data are representative of two independent experiments and displayed as mean ± SEM. Statistical analysis: 2-way ANOVA, significance designated for MA-BCN vs free MA. (**E-G**) hCD1Tg mice were IN vaccinated with selected nanoparticles and CellTrace Violet-labeled DN1 T cells were adoptively transferred the next day. After 1 week, DN1 T cell activation and proliferation was measured. **(E)** Representative FACS plots of DN1 T cells in the LN. Percentage of proliferating (**F**) and CD44-expressing **(G)** DN1 T cells in the LN and lung. Data represented as mean ± SEM. Statistical analysis: 2-way ANOVA. *p<0.05, **p<0.01, ***p<0.001, ****p< 0.0001.

Fig. 3. Vaccination with MA-BCN leads to antigen persistence 6 weeks post-vaccination. hCD1Tg mice were IT vaccinated with MA-BCN or BCN. 6 weeks later, CellTrace-labeled p25 and DN1 T cells were adoptively transferred, and T cell activation was measured after 1 week. **(A)** Experimental design. **(B)** Representative FACS plots of p25 and DN1 T cells in the LN. Percentage of proliferating **(C)** and CD44-expressing **(D)** p25 and DN1 T cells in the LN, lung, and spleen. N = 3 or 6 per condition. Outliers were identified through Grubbs method with alpha=0.05 with one sample removed.

884 Data represented as mean ± SEM. Statistical analysis: 2-way ANOVA. *$p < 0.05$, **$p < 0.01$, ***$p <$
885 0.001, ****$p < 0.0001$.
886
887 **Fig. 4. Ag85B and MA dual loaded BCNs activate antigen-specific T cells without Ag85B**
888 **persistence. (A)** DLS analysis of blank BCN and Ag85B-MA-BCN. (**B-D**) hCD1Tg mice were IT
889 vaccinated with Ag85B-MA-BCN or BCN and CellTrace-labeled p25 and DN1 T cells were
890 adoptively transferred the next day. After 1 week, T cell activation and proliferation was measured. **(B)**
891 Representative FACS plots of p25 and DN1 T cells in the LN. Percentage of proliferating (**C**) and
892 CD44-expressing (**D**) p25 and DN1 T cells in the LN, lung, and spleen (N = 4 or 5). (**E-G**) hCD1Tg
893 mice were IT vaccinated with blank BCN or Ag85B-MA-BCN. 6 weeks later, CellTrace-labeled p25
894 and DN1 T cells were adoptively transferred, and T cell activation was measured after 1 week. **(E)**
895 Representative FACS plots of p25 and DN1 T cells in the LN. **(F)** Percentage of proliferating p25 and
896 DN1 T cells**. (G)** Percentage of CD44-expressing p25 and DN1 T cells in the LN and lung. (N = 4).
897 Data represented as mean ± SEM. Statistical analysis: 2-way ANOVA. ns = not significant, *p<0.05,
898 **p<0.01, ***p<0.001, ****p< 0.0001.
899
900 **Fig. 5. Route of vaccination or vector type do not affect antigen persistence.** hCD1Tg mice were
901 IT vaccinated with MA or MA-BCN pulsed BMDCs at 6 weeks or 1 week prior to the adoptive
902 transfer of CellTrace-labeled DN1 T cells. T cell activation and proliferation was measured 1 week
903 after adoptive transfer. **(A)** Experimental design. **(B, C)** Percentage of proliferating **(B)** and CD44-
904 expressing **(C)** DN1 T cells in the LN, lung, and spleen of vaccinated mice. N = 4 per condition. N = 4
905 per condition. hCD1Tg mice were vaccinated SC (subcutaneously) or IV (intravenously) with blank
906 BCN, MA-BCN, or attenuated Mtb strain and 6 weeks later CellTrace-labeled DN1 T cells were
907 adoptively transferred. **(D)** Representative FACS plots of DN1 T cells in the LN of mice vaccinated
908 with indicated conditions. **(E)** Percentage of proliferating DN1 T cells and **(F)** Percentage of CD44-
909 expressing DN1 T cells in the LN and spleen of mice vaccinated with Blank-BCN (SC), MA-BCN (IV
910 and SC), and attenuated Mtb. N = 3-5 per condition. Data represented as mean ± SEM. Statistical
911 analysis: 2-way ANOVA. ns = not significant, *p<0.05, **p<0.01, ***p<0.001, ****p<0.0001.

Fig. 6. Persistent MA remains in part due to encapsulation inside alveolar macrophages and activates T cells through DCs. B6 or hCD1Tg mice were IT vaccinated with BCN loaded with a hydrophobic fluorescent dye (DiD) at 6 weeks, 6 days, 48 hours, 24 hours, or 4 hours prior to the experiment. LN, lung, and spleen were analyzed using **(A)** In Vivo Imaging System (IVIS). Single cell suspension was then obtained and presence of DiD BCN was quantified in **(B)** total lung, and **(C)** $CD45^-$ cells, neutrophils ($Ly6G^+$), alveolar macrophages ($CD11c^+SiglecF^+$), DCs ($CD11c^+$), monocytes ($CD11b^+CD11c^-$), B cells ($CD19^+$), T cells ($CD3^+$), NK cells ($NK1.1^+$), eosinophils ($CD11c^-SiglecF^+$) by flow cytometry. Gating strategy exemplified in **Suppl Fig 4**. hCD1Tg mice were IT vaccinated with either BCN or MA-BCN. After 6 weeks, alveolar macrophages were enriched from lungs using anti-SiglecF. Enriched or flow through cells were co-cultured with DN1 T cells in the presence or absence of hCD1Tg-expressing BMDCs for 48 hours, and DN1 T cells activation was measured. **(D)** Experimental design. **(E)** Percentage of CD25-expressing DN1 T cells. Data represented as mean ± SEM. Statistical analysis: 2-way ANOVA. ns = not significant, *p<0.05, **p<0.01, ***p<0.001.

Fig. 7. **MA-BCN vaccination leads to DN1 T cell differentiation into T follicular helper-like T cells**. Mixed bone marrow chimeric mice were created by adoptive transfer of DN1 bone marrow and congenic CD45.1 hCD1Tg bone marrow to irradiated hCD1Tg mice. After 5 weeks, mice were vaccinated with either MA-BCN or PBS, and DN1 surface marker expression was monitored in the blood and in organs at 6 wks. **(A)** Experimental design. **(B)** Percent $CD44^+$ DN1 T cells in the blood at various time points post vaccination. **(C)** Percent $CD44^+CD62L^+$ DN1 T cells in indicated organs at 6 weeks post vaccination. Memory ($CD44^+CD62L^+$) and naïve ($CD44^-CD62L^+$) DN1 T cells were sorted from MA-BCN vaccinated hCD1Tg-DN1 BM chimeras at 6 weeks post vaccination and subjected to RNAseq analysis. N=3 per condition **(D, E)** PCA of log fold change of gene expression for each T cell subset was performed relative to internal naïve T cell control. **(F)** Relative expression of key T_{FH} cell and DEGs in memory subset. **(G)** Gene enrichment analysis of upregulated DEGs was performed using Metascape. **(H)** Representative FACS plots of DN1 T cells in the LN of mice. Percentage of **(I)** $CXCR5^+PD1^+$ or **(J)** $KI67^+$ DN1 T cells DN1 T cells in LN, lung, and spleen. N = 3-5 per condition.

940 Data represented as mean ± SEM. Statistical analysis: 2-way ANOVA. *p<0.05, **p<0.01, ****p <

941 0.0001.

942

Figure 1

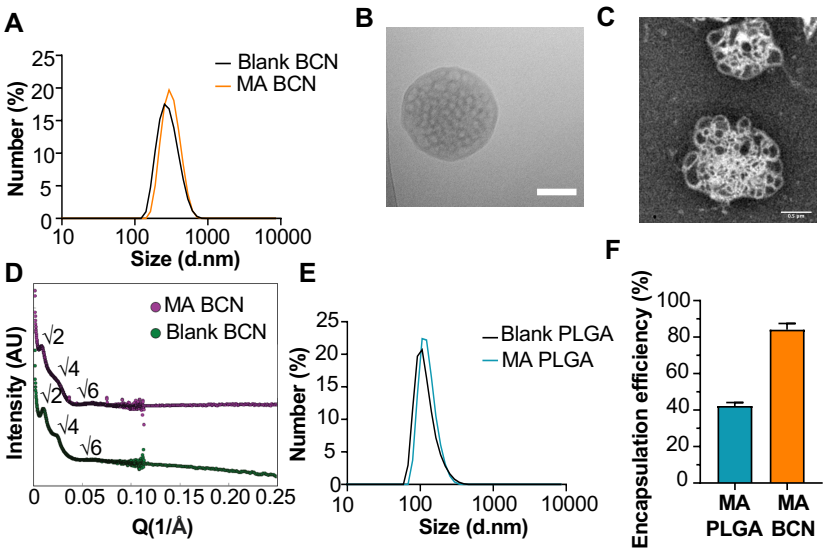

Figure 2

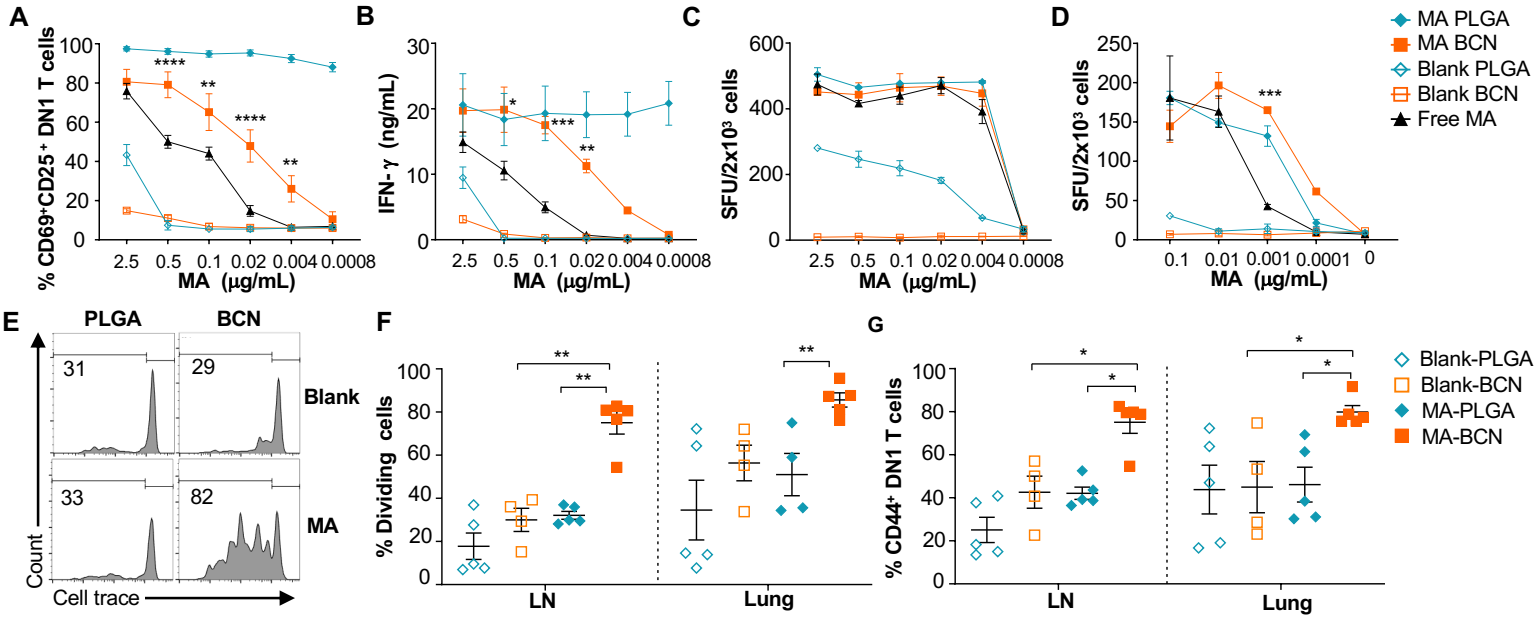

Figure 3

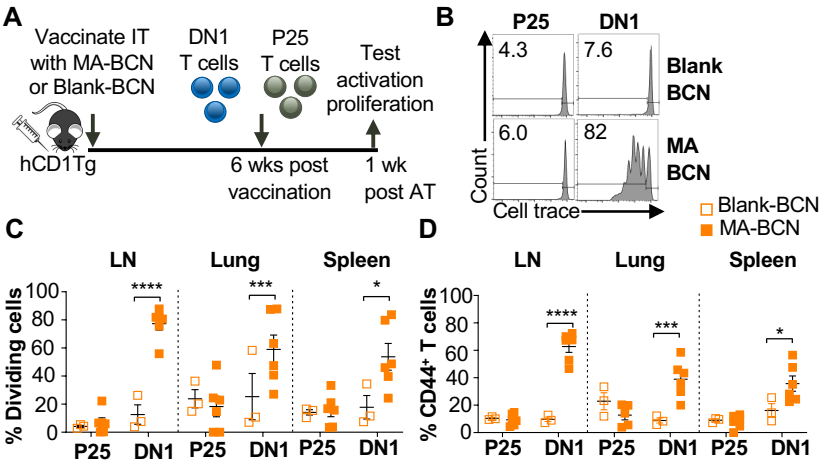

Figure 4

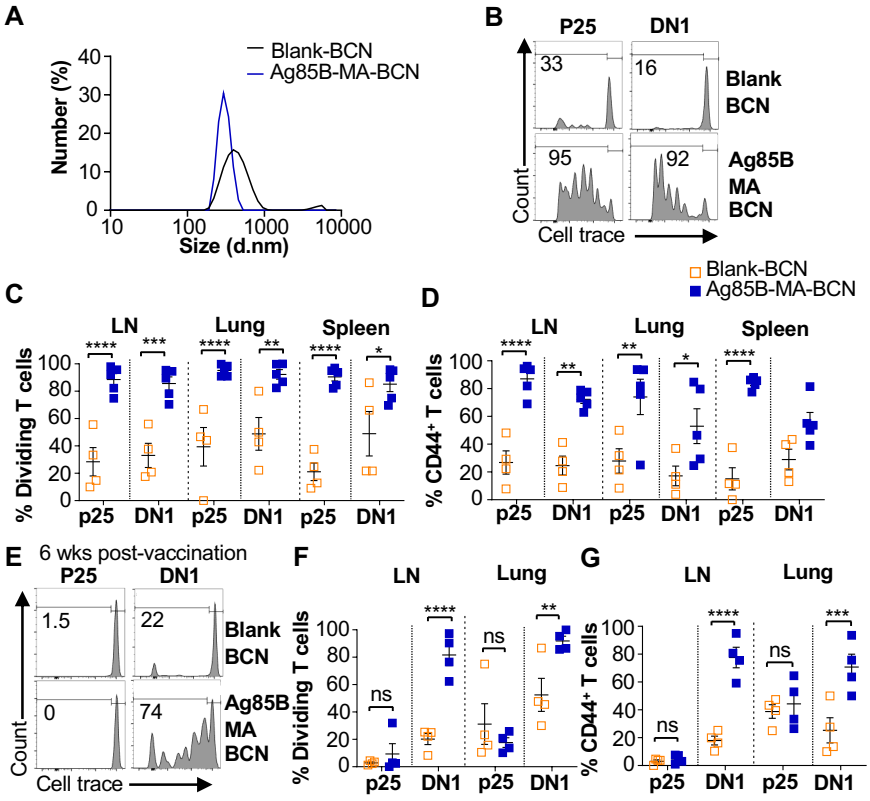

Figure 5

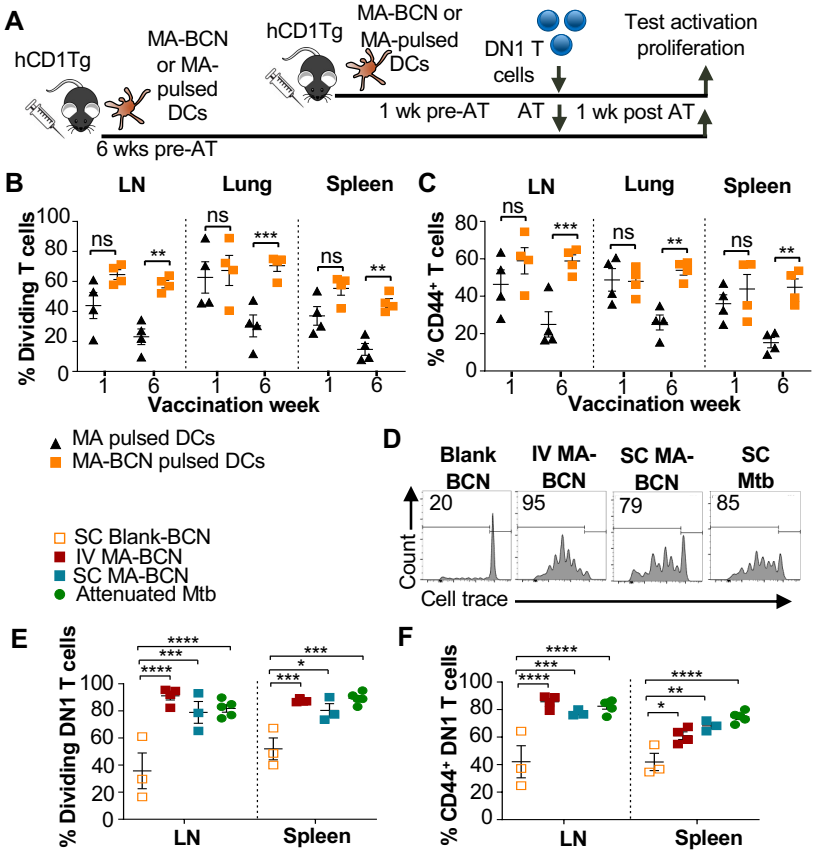

Figure 6

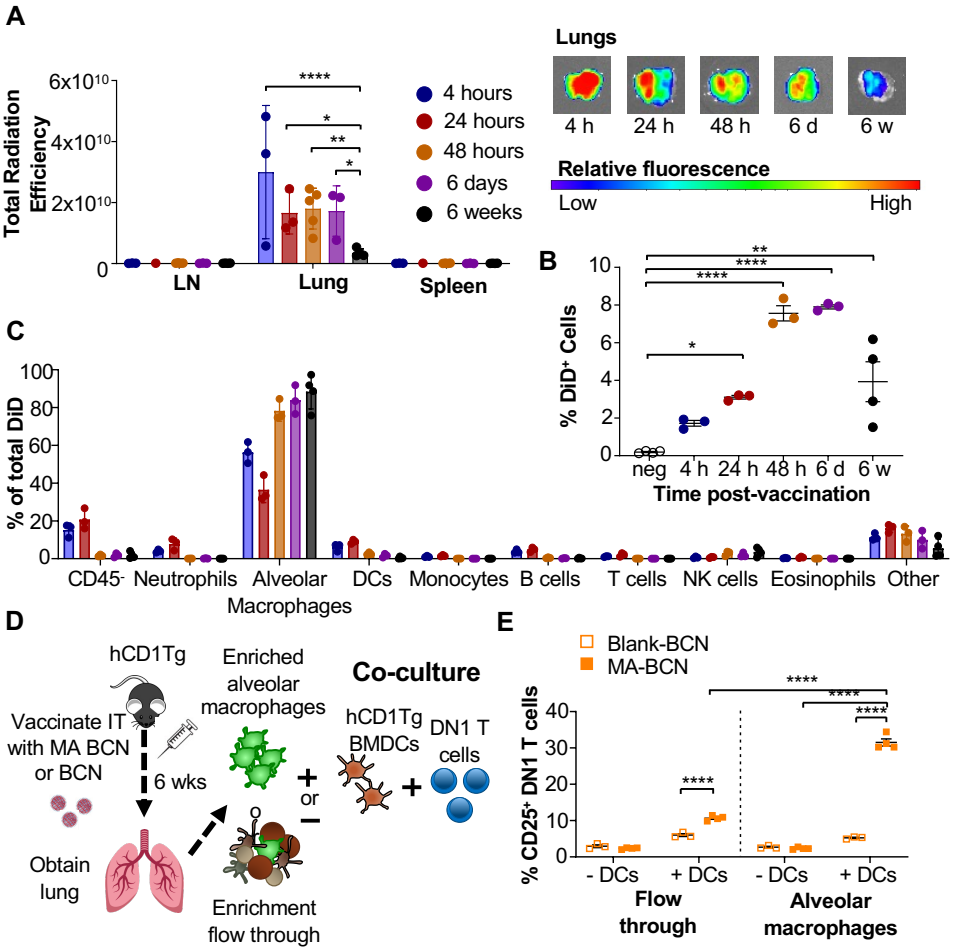

Figure 7